A Robot Joint With Variable Stiffness Using Leaf Springs

Junho Choi, *Member, IEEE*, Seonghun Hong, *Student Member, IEEE*, Woosub Lee, Sungchul Kang, *Member, IEEE*, and Munsang Kim, *Member, IEEE*

***Abstract*—Interaction with humans is inevitable for service robots, which results in safety being one of the most important factors in designing the robots. Compliant component is an answer to the safety issue at the cost of performance degradation. In order to reduce the performance degradation, manipulators equipped with variable stiffness have been studied by many researchers. This paper presents a variable stiffness joint (VSJ) designed for a robot manipulator, as well as a control scheme to control the stiffness and position of the VSJ. Compliance is generated by leaf springs and two actuators are used to control the position and stiffness of the joint using four-bar linkages. Two actuators in parallel configuration are connected to the spring. Changing the effective length of the spring results in a change in stiffness. The position of the joint is controlled via two actuators rotating at the same speed in the same direction. A nonlinear controller is used to control the VSJ, and a singular perturbation model is adopted to prove the stability of the closed-loop system. Experiments are conducted to show that the position and stiffness are controlled independent of each other, and having less stiffness at the joint helps in making an unexpected collision with an object safer.**

***Index Terms*—Actuators, service robots, variable stiffness.**

I. Introduction

SERVICE robots designed for daily chores at home require different design approaches than industrial robots to ensure physical safety. For traditional industrial robots, safety of a human operator is ensured by segregating work spaces of the human operator and the robots, whereas it is difficult to segregate the work space of the service robots and humans since the task requires the robots to share the work space with humans.

In order to address the safety problem of service robots, introducing compliance to the joints of the robots has been studied. Active compliance is mimicking mechanical compliance using actuators and sensor data. In [1], a robot with rigid joints was controlled to exhibit compliant motion using force feedback. Deflections in Cartesian coordinate and orientation of the end-effector were determined by the force and torque sensor data and compliance gain. In [2], distributed macro–mini actuation was used with different actuator characteristics. A large actuator was used for high-torque and low-frequency movement, while low-torque and high-frequency movement was covered by a small actuator. In order to reduce inertia of the manipulator, the large motor was located at the base of the manipulator, and the small motor was placed at the joint. For more compact design, a pneumatic actuator was used for low frequency bandwidth in [3].

When the sensors failed or sampling frequency was low, active compliance becomes unreliable to ensure safety of the humans, which was pointed out by Wang *et al.* [4], where a comparison study was conducted. Moreover, without any sensor failure or with high sampling frequencies, mechanical or electrical bandwidth of the system might prevent securing the safety of humans from unexpected collisions. Since active compliance is limited in ensuring the manipulator to remain safe, passive compliance has been paid much attention due to its reliability when safety is a primary concern. For various designs of actuators with passive compliance, see [5] and references therein.

Introducing compliance, however, poses a control problem, which has been studied by many researchers. Bicchi *et al.* investigated a robot joint with nonlinear springs and the control problem associated with the mechanical compliance in [6]. Feedback linearization was used to control a joint with constant compliance in [7] and joints with variable stiffness in [8] and [9]. Tomei used a proportional–derivative (PD) controller and proved the stability of the joint with a compliance in [10]. Spong [11] presented two different methods in controlling a joint with elasticity, which were using feedback-linearization method and forming the dynamics as a singularly perturbed system.

In order to realize an actuator with passive compliance, a series elastic actuator (SEA) was introduced in [12]. The SEA had advantages of low-pass-filtering shocks from and to the actuator and changing the force-control problem to the position-control problem. However, compliance due to the spring causes position inaccuracy and lower bandwidth. Adjustable compliance alleviates these problems. One way to realize adjustable compliance is to change the pretension of the spring connected to the motor. In [13], an additional moment arm and a motor were used to generate and control compliance. In [14], a nonlinear spring was realized with spiral pulleys and linear springs. The actuator was designed for a joint of a robot to help the robot to

Manuscript received February 23, 2010; revised August 24, 2010; accepted December 13, 2010. Date of publication January 20, 2011; date of current version April 7, 2011. This paper was recommended for publication by Associate Editor E. Guglielmelli and Editor K. Lynch upon evaluation of the reviewers' comments. This work was supported by the Intelligent Robotics Development Program, which is one of the 21st Century Frontier R&D Programs funded by the Ministry of Knowledge Economy of Korea.

J. Choi, W. Lee, S. Kang, and M. Kim are with the Center for Cognitive Robotics Research, Korea Institute of Science and Technology, 136-791 Seoul, Korea (e-mail: junhochoi@kist.re.kr; robot@kist.re.kr; kasch@kist.re.kr; munsang@kist.re.kr).

S. Hong is with the Center for Cognitive Robotics Research, Korea Institute of Science and Technology, 136-791 Seoul, Korea, and also with Hanyang University, 133-791 Seoul, Korea (e-mail: weluxmea@kist.re.kr).

Color versions of one or more of the figures in this paper are available online at http://ieeexplore.ieee.org.

Digital Object Identifier 10.1109/TRO.2010.2100450

walk. In [15], a cam disk and rollers pressed by linear springs were used. By controlling the pressing force from the spring, the stiffness was varied. In these designs, one compliant component and two motors were required. The stiffness and position of the joint were controlled independently by each motor. However, it was not possible for the joint to become completely stiff.

Another way is to change the effective length of the spring. Hollander *et al.* [16] used a helical spring and controlled the number of effective coil to change stiffness. Since changing the number of effective coil changed the effective length of the spring as well as the stiffness, it was not possible to control the stiffness and position of the joint independently. In [17], a mechanical-impedance adjuster was designed for a robot manipulator. A leaf spring was used to generate compliance at the joint. Using lead–screw mechanism, the effective length of the spring was changed, which caused the stiffness of the joint change. In these designs, it was possible for the joint to be rigid. However, the motor and the device to change the stiffness became an additional load to the motor to control the position since they were connected in series.

Actuators in parallel configuration have advantage over actuators in series since the load of the joint is shared by the actuators. Two motors with nonlinear springs antagonistically connected result in a joint with adjustable compliance. To realize a nonlinear spring, rolamite springs were used in [18]. The shapes of the springs were designed so that the stiffness of the spring became nonlinear. With nonlinearity of the spring, stiffness of the joint was variable. In [19], rollers and a frame were used to implement a nonlinear spring. Tonietti *et al.* used a timing belt and linear springs to realize nonlinear springs in [20]. Since the power of the motors was transmitted through the timing belt, the strength of the belt limited the maximum allowable payload. The existence of the idle pulley made the joint bulky. To overcome such disadvantages, another design was presented in [21]. The presented VSA-II used a four-bar linkage system to transmit the power, which showed more robustness and larger load-bearing capability. In these antagonistic designs, two motors and two springs were used to control the stiffness and position. Rotation of the motors with relative angle of the motors unchanged made the link rotate. When the relative position of the motors varied with the mean position of motors unchanged, the stiffness of the actuator was changed. In order to hold a constant stiffness, the motors need to apply torque, which implies poorer energy efficient.

Preliminary concept of the variable stiffness joint (VSJ) was presented in [22] without control method and proof of the stability. In this paper, the control method, as well as the design of the VSJ, is presented. In Section II, design of the VSJ is explained. The VSJ has two identical actuators connected to leaf springs. Compliance is generated by the leaf springs whose effective length is controlled by the actuators via four-bar linkage. Instead of one actuator becoming an additional load to the other actuator, two actuators evenly share the load of the joint, which results in better energy consumption. In addition, the four-bar linkage makes the VSJ more energy efficient since it is not required to apply additional torque in order to hold stiffness, as discussed in [23], where energy consumption of various actuators with adjustable passive compliance were compared. It was shown that having to apply torque to hold a constant stiffness was a reason of higher energy consumption. In Section III, a control method is introduced. Each actuator is controlled by a velocity controller, and the link is controlled via full state feedback. The dynamics of the VSJ is formed as a singularly perturbed system. The stability of the VSJ with the controller is shown using a Lyapunov function. In Section IV, the result of the experiment is presented. To show the effect of the variable stiffness of the VSJ, an experiment of hitting balls with different stiffness are presented. When the stiffness is maximum, balls that are hit by the link of the VSJ fly farther than minimum stiffness. The experiment shows that the acceleration of the balls after collision with the link is smaller when the stiffness is small, which implies that the collision is safer. The conclusion is made in Section V.

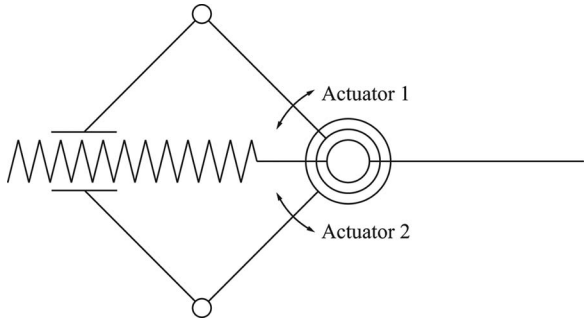

Fig. 1. Schematics of the VSJ. Leaf springs are attached to the axis, and the effective length of the spring is varied by four-bar linkages, which are actuated by two identical actuators.

II. Design of the Variable Stiffness Joint

The design of the VSJ is presented in this section. The main concept of the VSJ is to have two identical "actuators" connected to a passive compliant component. Each actuator consists of a harmonic gear and an electrical motor. Passive compliance is variable for safer manipulation with minimum performance degradation. Compliance is generated by leaf springs. Changing the effective length of the springs results in stiffness change. In order to change the effective length of the springs, a four-bar linkage system is used (see Fig. 1).

Note that the compliance component is located in series with the actuators, whereas the actuators are in parallel configuration. Due to the parallel configuration of the actuators, the load to the joint is evenly distributed to each actuator, whereas one actuator becomes an additional load to the other in case of series actuation. Furthermore, since compliance is generated by the leaf spring and the actuators control the effective length of the leaf springs, no power is necessary to hold the stiffness, which implies that the VSJ is more energy efficient. Since it is not necessary to use an additional mechanism to change stiffness (i.e., lead screw), a simpler design is possible. As the slider moves toward to the axis of rotation, the effective length of the spring becomes zero, which implies that the VSJ becomes a rigid actuator.

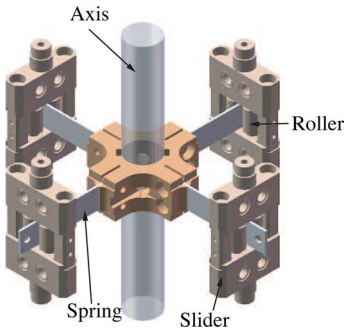

Fig. 2. Axis with four identical springs attached. The sliders move along with the springs with the rollers inside of the sliders.

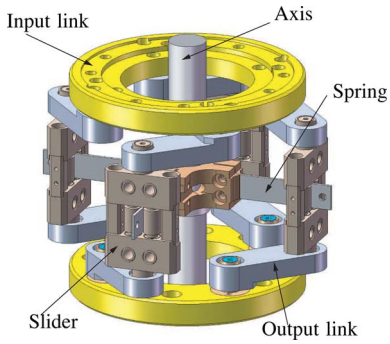

Fig. 3. Link a is attached to the actuators and rotates about the axis. The slider is connected to the link b, whose other end is connected with link a. The springs are attached to the axis so that the axis rotates when the sliders rotate.

A. Generating Compliance With Leaf Spring

Compliance of the VSJ is generated by N leaf springs, which are attached to the axis. The springs are separated by $360/N$ degrees. One end of each spring is attached to the axis and the other end remains free so that the spring bends with an external force applied to the spring. Two rollers, which are contained in a frame called "slider," roll on each side of the spring (see Fig. 2). Effective length of each spring is determined by the position of the slider in the radial direction. The upside and downside of each slider are held by two links, which are called "output links" of a four-bar linkages. A link that is connected to each actuator is called a "Input link." The input links are designed to be a circular frame, which are connected to the harmonic gears of the actuators (see Fig. 3).

The four-bar linkage transforms rotation into translational movement and determined the position of the slider. With the relative position of the actuators being unchanged, the effective length of the spring remain unchanged. Then, the VSJ acts as an actuator with constant compliance connected in series. Fig. 4 shows the assembled VSJ. The guides prevent the sliders from being distorted due to the applied torque at the axis.

Stiffness of each spring is calculated using the position of the slider and dimension of the spring (see Fig. 5).

Let D be the diameter of the axis and let l be the distance to the slider from the axis. When an external torque is applied, the springs bend due to the torque and angular displacement of the axis. Letting dF_i be the force applied to ith slider due to the external torque, then the force is given as follows:

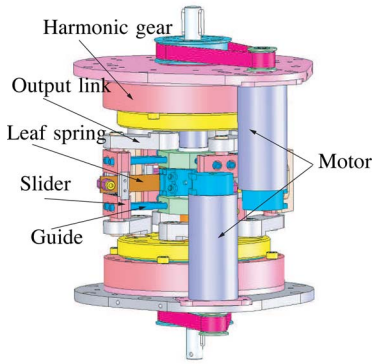

Fig. 4. Assembled VSJ with four springs. The guide prevents the pivot from being twisted by applied torque.

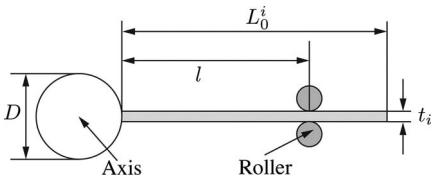

Fig. 5. Schematic of ith leaf spring with rollers. When the rollers slide on the leaf spring, the effective length of the spring changes, which is the distance between the axis and the rollers. Change of the effective length of the spring results in changing stiffness.

$$dF_i = \frac{\sigma_i d\theta}{l + (D/2)}, \qquad i = 1, \ldots, N \tag{1}$$

where σ_i is torsional stiffness of each spring, dF_i is the force at each slider due to the torque, and $d\theta$ is the angular displacement of the axis. Note that the amount of bent is the same for each spring since all the springs are attached to the axis and that the positions of the sliders are identical. Then, the displacement of the slider in angular direction is approximated as

$$d\delta = (l + D/2)d\theta. \tag{2}$$

Letting L_0^i be the length of ith spring, w_i be the width of the spring, and t_i be the thickness of the spring, then following the development in [24], the force to the slider is given as follows:

$$dF_i = \frac{E_i w_i t_i^3}{4l^3} d\delta \tag{3}$$

where E_i is the Young's modulus of each spring. Therefore, with (1)–(3), the stiffness of the joint is given as

$$\sigma_i = (l + D/2)\frac{dF_i}{d\theta} = (l + D/2)^2 \frac{E_i w_i t_i^3}{4l^3}. \tag{4}$$

The stiffness of the joint is given as

$$\sigma = \sum_{i=1}^{N} \sigma_i = \sum_{i=1}^{N} (l + D/2)^2 \frac{E_i w_i t_i^3}{4l^3}. \tag{5}$$

Note that stiffness of the VSJ is determined by the shape and material of the leaf spring. Since stiffness depends on the shape of the spring, it is possible to design stiffness of the VSJ by designing the leaf spring, i.e., rectangular shape, tapered shape,

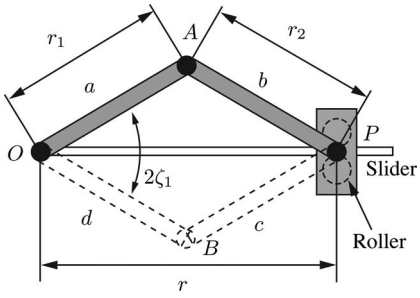

Fig. 6. Schematics of linkages connected at the slider. The link a and d are attached to both actuators. All the joints of the four-bar system are revolute joints. The slider is connected to the link b and c so that it is possible for the slider to rotate freely.

etc. However, the range of stiffness function obtained by designing the spring is limited. For simplicity, a rectangular shape is chosen in this paper.

B. Changing the Stiffness

In order to change the stiffness, it is necessary to change the positions of the sliders in radial direction. The positions of the sliders are changed by changing the relative positions of two input links of the four-bar linkages. All the joint of the four-bar system are revolute joints (see Fig. 6). Two output links that are connected to a slider have the same length. The other two links are input links and have the same length. Each input link is attached to each actuator.

The point O is located at the center of the rotational axis. The input links are denoted by a and d, respectively. The output links are denoted by b and c. Let r_1 be the length of the links a and d, and let r_2 be the length of the links b and c. Letting $2\zeta_1$ be the angle between the links a and d, then, the distance to the slider from the point O, which is denoted by r, is given as follows:

$$r = r_1 \cos\zeta_1 + \sqrt{r_2^2 - r_1^2 \sin^2\zeta_1} \tag{6}$$

where $r > 0$, and $0 < \zeta_1 < \pi/2$. Since the input links rotate around the axis, the distance to the slider becomes $r = l + D/2$ (see Fig. 5). The torsional stiffness is calculated using (5) and (6) as follows:

$$\sigma(\zeta_1) = \frac{(r_1\cos\zeta_1 + \sqrt{r_2^2 - r_1^2\sin^2\zeta_1})^2}{(r_1\cos\zeta_1 + \sqrt{r_2^2 - r_1^2\sin^2\zeta_1} - \frac{D}{2})^3} \sum_{i=1}^{N} \frac{E_i w_i t_i^3}{4} \tag{7}$$

where $\sigma(\zeta_1)$ is an invertible function for $0 < \zeta_1 < \pi/2$. Note that as ζ_1 increases, the effective length of the spring becomes zero. Then, the VSJ becomes a rigid joint.

Let q_1 and q_2 be the position of each actuator. Since the link a and d are attached to each actuator, ζ_1 is given as follows:

$$\zeta_1 = \frac{q_1 - q_2}{2}. \tag{8}$$

Since stiffness of the VSJ depends on the effective length of the leaf spring, which is determined by the location of the slider in the radial direction, controlling the position of the slider in the radial direction is equivalent to controlling the stiffness. Equation (6) shows that the location of the slider in radial direction is a function of the relative angle between the actuators, which is denoted $2\zeta_1$ in Fig. 6. The location of the slider in angular direction, however, is the rest position of the spring. Since the four-bar linkage system is symmetric, the rest position of the slider is given as follows:

$$\zeta_2 = \frac{q_1 + q_2}{2} \tag{9}$$

where q_1 and q_2 are the positions of the actuators.

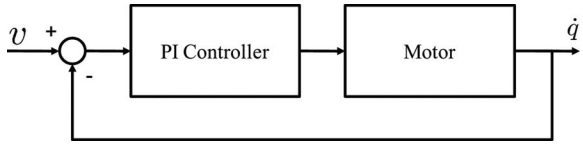

Fig. 7. Controller of each actuator. The velocity of each controller is controlled using the PI controller.

III. Controlling the Variable Stiffness Joint

The velocity of each actuator is controlled by a proportional-integral (PI) controller (see Fig. 7).

The response of the PI controller is faster than other controller so that it is assumed that the velocity of the actuator reaches the desired velocity instantaneously. Then, the dynamics of the VSJ, including the velocity controllers, is given as follows:

$$\begin{cases} \dot{q}_1 = v_1 \\ \dot{q}_2 = v_2 \\ \ddot{q}_3 = -\frac{\sigma((q_1-q_2)/2)}{J_l}(q_3 - \frac{q_1+q_2}{2}) \end{cases} \tag{10}$$

where q_3 is the position of the link, J_l is the moment of inertia of the link, $\sigma((q_1 - q_2)/2)$ is the stiffness generated by the leaf spring, and v_1 and v_2 denote the velocity command to each actuator, respectively. Since $(q_1 + q_2)/2$ is the rest position of the leaf spring, and q_3 is the position of the link, the difference is the deflection of the leaf spring.

Let us define a coordinate transform T as follows:

$$\begin{bmatrix} \zeta_1 \\ \zeta_2 \\ \zeta_3 \end{bmatrix} = \begin{bmatrix} 1/2 & -1/2 & 0 \\ 1/2 & 1/2 & 0 \\ 0 & 0 & 1 \end{bmatrix} \begin{bmatrix} q_1 \\ q_2 \\ q_3 \end{bmatrix} = T \begin{bmatrix} q_1 \\ q_2 \\ q_3 \end{bmatrix}. \tag{11}$$

Then, the dynamics of the VSJ in ζ coordinates becomes

$$\begin{cases} \dot{\zeta}_1 = u_1 \\ \dot{\zeta}_2 = u_2 \\ \ddot{\zeta}_3 = -\frac{\sigma(\zeta_1)}{J_l}(\zeta_3 - \zeta_2) \end{cases} \tag{12}$$

where $u_1 = (v_1 - v_2)/2$, and $u_2 = (v_1 + v_2)/2$.

Letting $K_f^p, K_s^p,$ and K_s^d be nonzero constants, then the control law of the VSJ is defined as follows:

$$u_1 = K_f^p(\zeta_1 - \zeta_1^d) \tag{13}$$

$$u_2 = K_s^p\zeta_2 - \frac{K_s^p}{2}\zeta_3 - \frac{K_s^p}{2}\zeta_3^d + K_s^d\dot{\zeta}_3 \tag{14}$$

where ζ_1^d and ζ_3^d are the desired relative position of the actuators and link position, respectively. In typical application of the VSJ, since it is typical that the VSJ is connected to a link, which

has bigger inertia than four-bar linkages and the actuators are shared to control the position and the stiffness of the VSJ, it is inevitable to control the position of the link slower than relative position of the actuators. It is assumed that $K_f^p = (1/\epsilon)K_s^p$ in (13), where ϵ is a small positive constant. Then, the dynamics of the closed-loop system becomes

$$\begin{cases} \epsilon\dot{\zeta}_1 = K_s^p(\zeta_1 - \zeta_1^d) \\ \dot{\zeta}_2 = K_s^p(\zeta_2 - \zeta_3) + \frac{K_s^p}{2}(\zeta_3 - \zeta_3^d) + K_s^d\dot{\zeta}_3 \\ \ddot{\zeta}_3 = -\frac{\sigma(\zeta_1)}{J_l}(\zeta_3 - \zeta_2). \end{cases} \tag{15}$$

The equilibrium point of (15) is $\zeta_1 = \zeta_1^d$, $\zeta_2 = \zeta_3 = \zeta_3^d$, and $\dot{\zeta}_3 = 0$. Letting $\zeta^f = \zeta_1 - \zeta_1^d$, and

$$\zeta^s = \begin{bmatrix} \zeta_2^s \\ \zeta_3^s \\ \dot{\zeta}_3^s \end{bmatrix} = \begin{bmatrix} \zeta_2 - \zeta_3^d \\ \zeta_3 - \zeta_3^d \\ \dot{\zeta}_3 \end{bmatrix} \tag{16}$$

then the dynamics of the closed loop system in the state space is given as

$$\epsilon\dot{\zeta}^f = K_s^p\zeta^f =: f_f(\zeta^f)$$

$$\dot{\zeta}^s = \begin{bmatrix} K_s^p(\zeta_2^s - \zeta_3^s) + \frac{K_s^p}{2}\zeta_3^s + K_s^d\dot{\zeta}_3^s \\ \dot{\zeta}_3^s \\ -\frac{\sigma(\zeta^f)}{J_l}(\zeta_3^s - \zeta_2^s) \end{bmatrix} \tag{17}$$

$$=: f_s(\zeta^f, \zeta^s) \tag{18}$$

with $\zeta_0^f = 0$, and $\zeta_0^s = [\,0, 0, 0\,]^T$ being the equilibrium point. Since $\zeta_0^f = 0$ is the unique solution to $f_f(\zeta^f) = 0$ when $K_s^p \neq 0$, $h(\zeta^s) := 0$ is the isolated equilibrium point of (17) for $\zeta^s \in \mathbb{R}^3$. Then, models (17) and (18) are in the standard form of singular perturbation. Following the standard approach in [25], the boundary-layer system is given as

$$\dot{\zeta}^f = f_f(\zeta^f) = K_s^p\zeta^f. \tag{19}$$

The reduced system is given as follows:

$$\dot{\zeta}^s = f_s(\zeta_0^f, \zeta^s) = \begin{bmatrix} K_s^p(\zeta_2^s - \zeta_3^s) + \frac{K_s^p}{2}\zeta_3^s + K_s^d\dot{\zeta}_3^s \\ \dot{\zeta}_3^s \\ -\frac{\sigma(\zeta_0^f)}{J_l}(\zeta_3 - \zeta_2) \end{bmatrix}. \tag{20}$$

Lemma 1. The boundary-layer system (19) is exponentially stable at $\zeta_0^f = 0$, if $K_s^p < 0$.

Proof: Letting $V_f = (1/2)(\zeta^f)^2$ be the candidate Lyapunov function, then, for all $\zeta^f \neq 0$, the derivative of the Lyapunov function is given by

$$\dot{V}_f = \zeta^f\dot{\zeta}^f = K_s^p(\zeta^f)^2 < 0. \tag{21}$$

Since the system is linear, the system is exponentially stable. ■

Note that the relative position of the actuators needs to be controlled within boundaries due to the limited range of movement. The boundaries are determined by the length of the four-bar linkages and the length of the leaf spring. When designing a reference trajectory for the relative position of the actuators, the reference needs to remain within the boundaries.

Lemma 2: Let λ be a positive constant, and let $\kappa_0 = \sigma(\zeta_0^f)/J_l$. Letting $K_s^p = -2\lambda$, and $K_s^d = -1 - (\lambda^2/\kappa_0)$, then the control law of the reduced system in (14) is a stabilizing control of the reduced system in (20). Moreover, the reduced system is exponentially stable.

Proof: For proof of Lemma 2, see the Appendix. ■

Theorem 1: Let u be a control law for the full model and defined as follows:

$$u = \begin{cases} u_1 = -\frac{2\lambda}{\epsilon}\zeta^f \\ u_2 = -2\lambda\zeta_2^s + \lambda\zeta_3^s - \left(1 + \frac{J_l\lambda^2}{\sigma(\zeta^f)}\right)\dot{\zeta}_3^s \end{cases} \tag{22}$$

where $\lambda > 0$, then the full model (12) with the controller (22) is exponentially stable.

Proof: $\zeta^f = 0$ is an isolated root of the equation $0 = f_f(\zeta^f)$. By Lemmas 1 and 2, the boundary-layer system and the reduced system are exponentially stable. Therefore, by [26, Th. 9.3], the system is exponentially stable. ■

Note that torque control of the VSJ is possible. Since the VSJ acts as an SEA in [12] when the stiffness is held constant, a simple approach is to change the force-control problem to a position-control problem. The torque generated by the leaf spring is given as

$$\tau = \sigma(\zeta_1)(\zeta_3 - \zeta_2). \tag{23}$$

When the link position is fixed at $\zeta_3 = \zeta_3^d$ and the relative position is fixed at $\zeta_1 = \zeta_1^d$, the desired rest position of the VSJ is calculated with (23) as follows:

$$\zeta_2^d = \zeta_3^d - \frac{\tau^d}{\sigma(\zeta_1^d)} \tag{24}$$

where τ^d is the desired torque, ζ_1^d is the desired relative position, and ζ_3^d is the position of the link. Then, it controls the relative position of the actuators and the rest position of the spring. Other methods are found in [27]–[29].

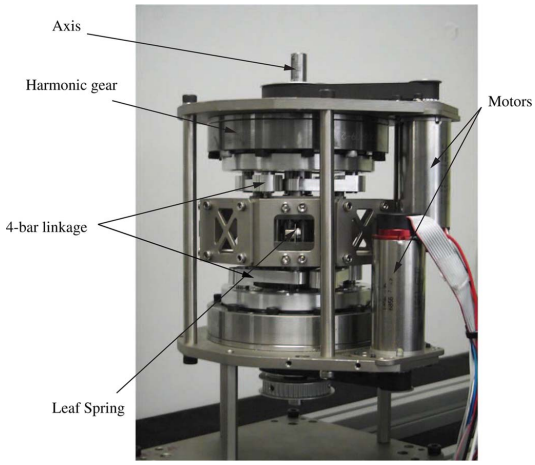

Fig. 8. Implemented VSJ. It consists of two identical motors and harmonic gears and four identical leaf springs and sliders.

IV. Experiment

In this section, results of experiments to evaluate the implemented VSJ are presented.

Fig. 8 shows the implemented VSJ. Two identical actuators are connected to the input links of the four-bar linkages. Each

TABLE I
MODEL PARAMETERS FOR THE VSJ AND EACH COMPONENT

Component	Parameters	unit	Value
VSJ	Max. Torque	Nm	30
	Mass	kg	4.95
	Diameter	mm	146
	Height	mm	144
Leaf Spring	Thickness	mm	1
	Width	mm	10
	Young's modulus	GPa	206
4-bar linkage	Input link (link a)	mm	33
	Output link (link b)	mm	36
Harmonic Gear	Mass	kg	0.91
	Gear Ratio	-	51:1
	Diameter	mm	110
Electric Motor	Mass	kg	0.271
	Power	Watt	200
	Speed (No load)	rpm	17000

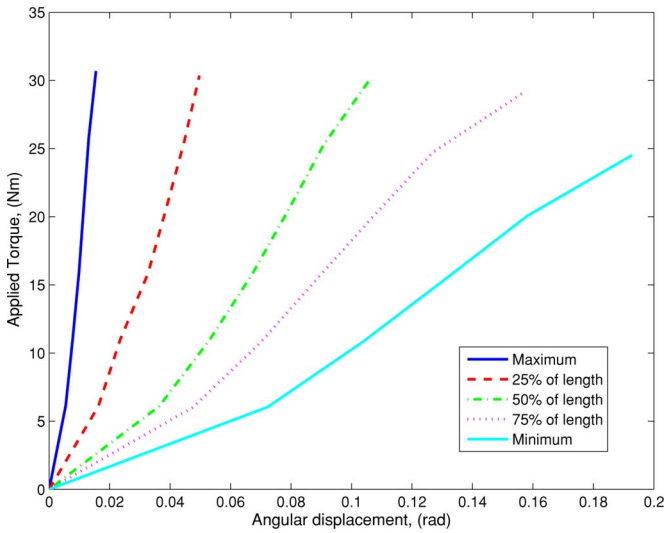

Fig. 9. Torque generated by the VSJ with different angular displacements.

actuator consists of a harmonic gear and an electrical motor. The electrical motor and the harmonic gear is connected through a timing belt with a 3:1 gear ratio. Since the gear ratio of the harmonic gear is 51:1, the overall gear ratio is 153:1. Four identical leaf springs are attached to the axis. Dimensions of the VSJ and other parameters are listed in Table I. The parameters are designed to meet the specification of the manipulator of a service robot.

A slider moves along each spring and the output links of the four-bar linkage are connected to the sliders. The rotation of the axis is measured by an encoder, while the rotation of the shaft of each motor is measured by another encoder attached to the shaft. Guides are used to prevent the sliders from being distorted due to the force at both ends of the sliders. When the four-bar system reaches out the most, the effective length of the spring is 26.3 mm. The VSJ is designed to generate $30\,\mathrm{N}\cdot\mathrm{m}$.

Fig. 9 shows the measured stiffness of the VSJ. In order to measure the stiffness, angular displacement of the axis is measured when known torque is applied at the axis.

Note that the angular displacement is almost linear with respect to the applied torque. Therefore, it is possible to approximate the stiffness with a constant when the relative position

TABLE II
TORSIONAL STIFFNESS OF THE VSJ

Relative position (rad)	Stiffness (Nm/rad)
0	252.16
0.0873	326.55
0.1745	511.35
0.2618	1064.50
0.3491	3647.90

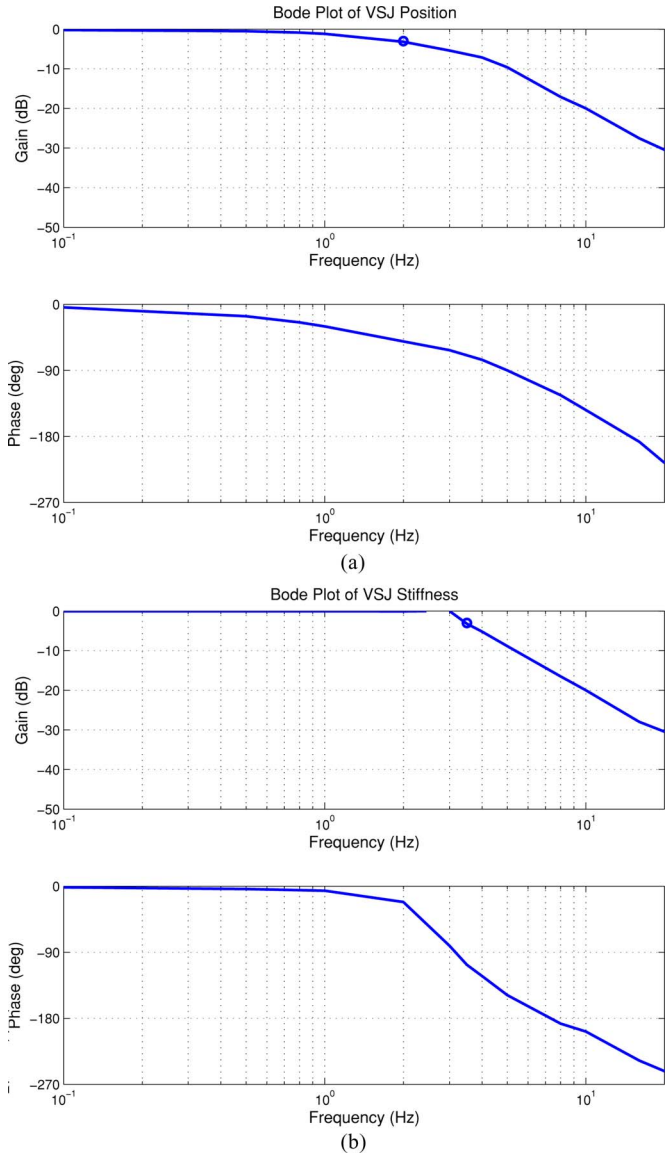

Fig. 10. Frequency response of the VSJ. (a) Frequency response of the position. Bandwidth of the position is 2 Hz. (b) Frequency response of the stiffness. Bandwidth of the stiffness is 3.5 Hz.

of the actuators is unchanged, which makes the controller simpler. Table II shows the approximated stiffness with different relative positions of the actuators. Maximum stiffness is about 3648 Nm/rad, and minimum stiffness is about 252 Nm/rad.

The result of frequency analysis is shown in Fig. 10. Magnitude and phase of the position and stiffness of the VSJ are measured when commands to the position and stiffness are sinusoidal functions with various frequencies. Fig. 10(a) shows the

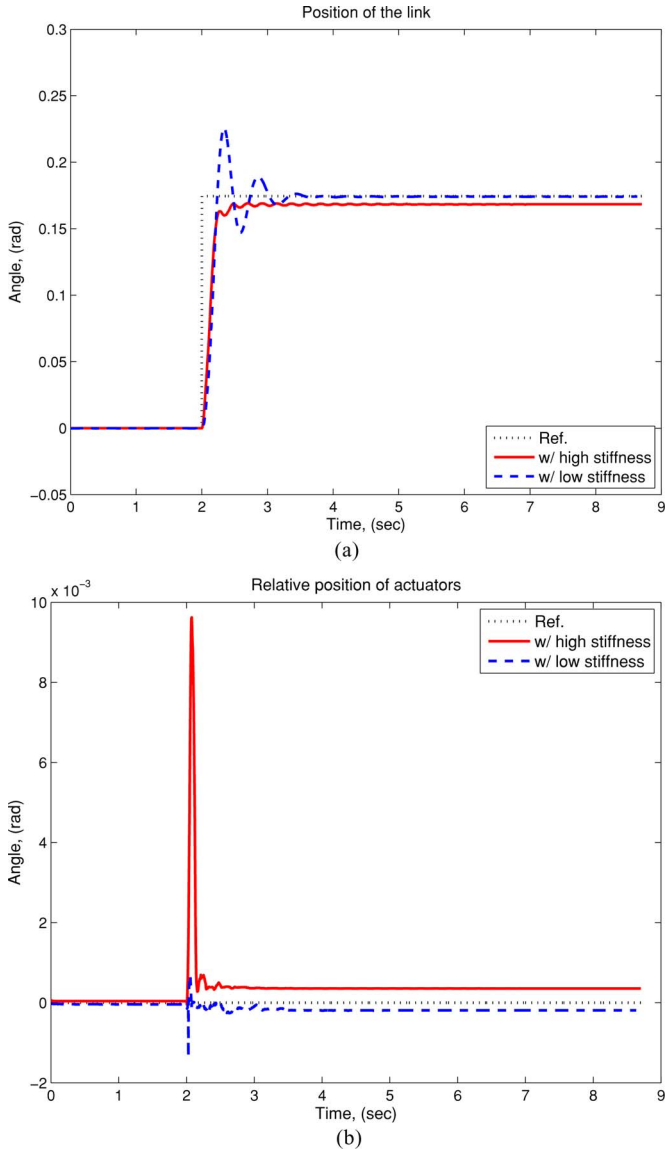

Fig. 11. Step response of the VSJ when the reference of the link position is a step function. (a) Position of the link, i.e., ζ_3, when the position command is a step function. (b) Angular displacement of two actuators, i.e., ζ_1.

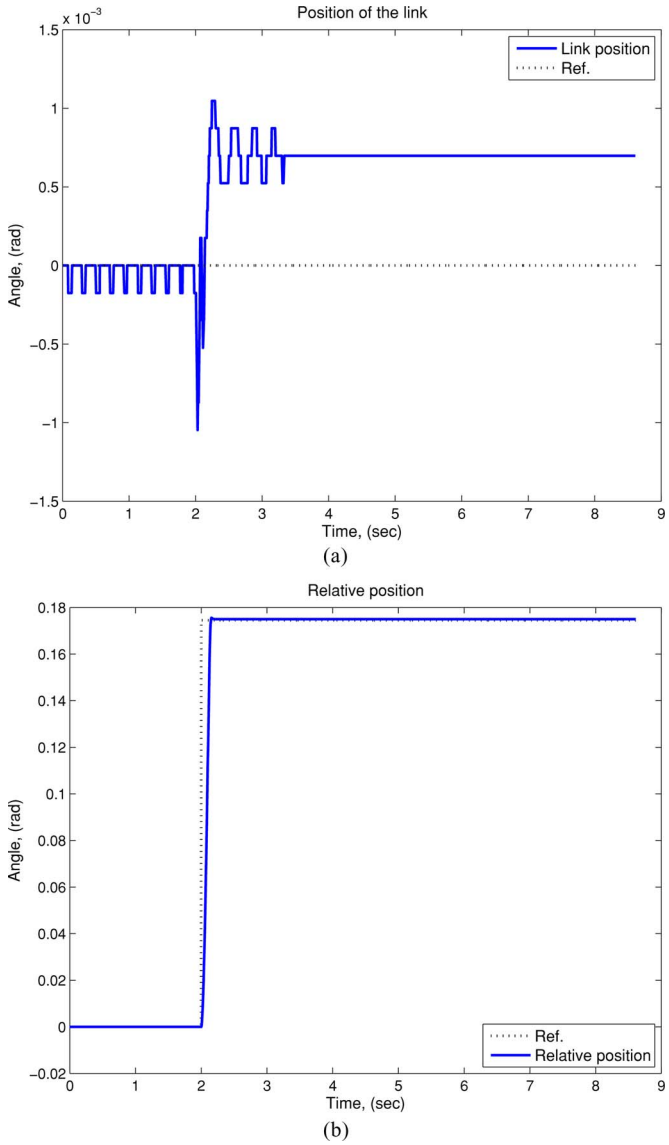

Fig. 12. Step response of the VSJ when the reference of the relative position of the actuator is a step function. (a) Position of the link, i.e., ζ_3, when the position command is a step function. (b) Relative position of two actuators, i.e., ζ_1.

frequency response of the position of the VSJ. The 3-dB cutoff frequency of the position is 2 Hz. Fig. 10(b) shows the frequency response of the stiffness. The 3-dB cutoff frequency of the stiffness is 3.5 Hz.

Responses to position commands with different stiffness are shown in Fig. 11. The relative position of the actuators, which is denoted by ζ_1 in (12), is controlled to be unchanged. A link, whose inertia is about 0.5 kg $\cdot$ m^2, is attached to the VSJ. Fig. 11(a) shows the position of the link, which is denoted by ζ_3 in (12), with different stiffness. When the stiffness is maximum, vibration does not occur, the rise time becomes 0.164 s, and the settling time is 0.475 s. However, when the stiffness is minimum, vibration due to the position command occurs. The rise time is 0.153 s, and the settling time is 1.133 s. Due to the vibration, the settling time is longer with minimum stiffness. Model uncertainty and friction cause steady-state error. Fig. 11(b) is the relative-position error when the position reference is a step function. The relative-position error remains less than 0.010 rad.

Fig. 12 shows the response of the VSJ when the reference function for the relative position is a step function, while the position of the link is controlled to remain unchanged. Fig. 12(a) shows the position error of the link. The position of the link, i.e., ζ_3, changed less than 0.015 rad. The changes in the link position are due to discrepancies in actuators, which are assumed to be identical. Fig. 12(b) shows the relative position of the actuators, i.e., ζ_1. The rise time is 0.093 s, and the settling time is 0.155 s. Note that larger control gain results in the rise and settling time of the relative position being less than the link position.

In Fig. 13, the response of the VSJ is shown when both position and stiffness of the VSJ are changed. Stiffness is changed

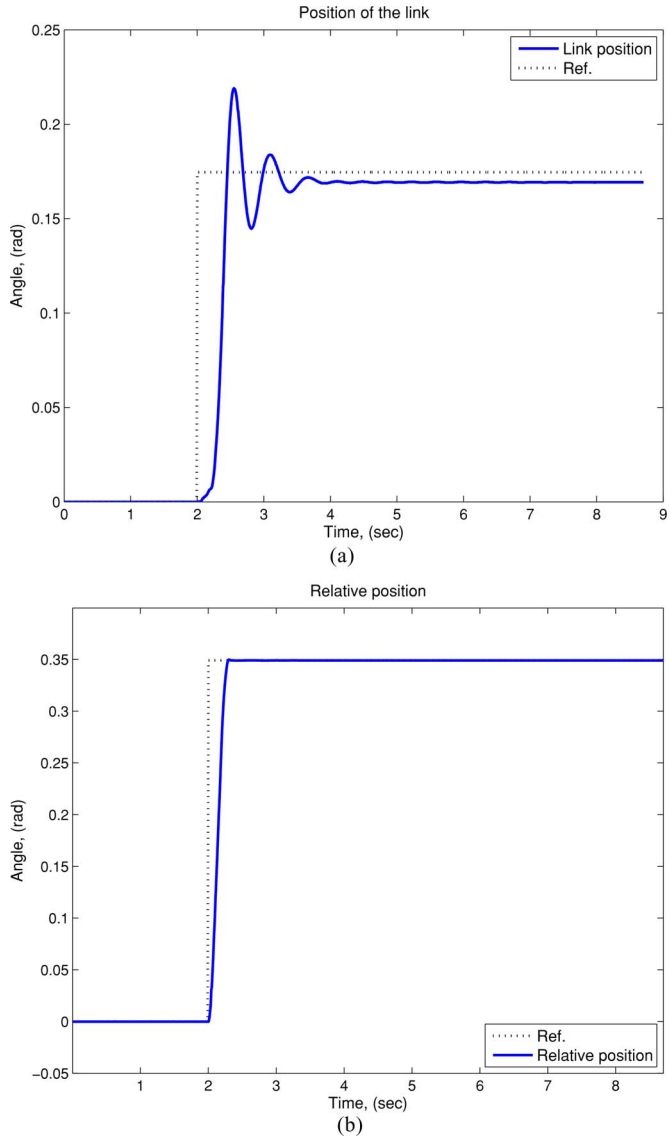

Fig. 13. Step response of the VSJ when unit step functions are applied as references for the position of the link and the relative position of the actuators. (a) Position of the link, i.e., ζ_3, when the position command is a step function. (b) Relative position of the actuators, i.e., ζ_1.

from its maximum value to minimum value within less than 0.3 s. Due to the inertia of the link, position response shows an overshoot similar to the step response of the link with minimum stiffness in Fig. 11(a).

Steady-state errors exist due to the friction and model uncertainties not included in the model.

In order to show the effect of the VSJ in unexpected collision, hitting a golf ball and a table-tennis ball experiment was conducted. A golf ball and a table-tennis ball are hit by the VSJ with different stiffness. A 520-mm-long link, which is made of aluminum, is attached to the axis of the VSJ. The balls are hit by the link at the height of 17 mm (see Fig. 14). The VSJ rotates with maximum and minimum stiffness at 1.2 rad/s. In order to reduce the effect of vibration due to the link, the VSJ rotates 1080° before hitting the ball when the stiffness is minimum.

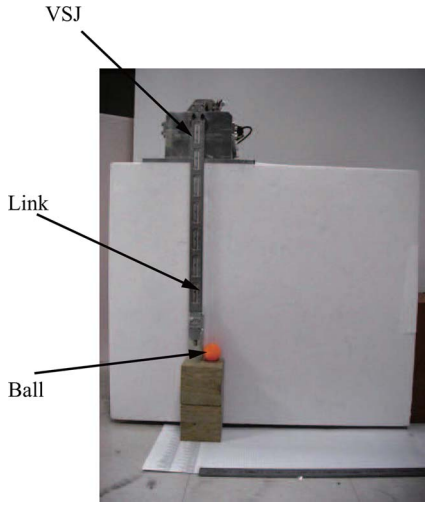

Fig. 14. Experimental setup for hitting-ball experiment. A link is attached to the VSJ and the link hits the ball on the stand.

TABLE III
FLIGHT DISTANCE OF THE BALLS HIT BY A LINK

Ball	Stiffness	Flight Distance
Golf ball	Maximum Stiffness	510 mm
	Minimum Stiffness	467 mm
Table-tennis ball	Maximum Stiffness	801 mm
	Minimum Stiffness	697 mm

Length of the link is 520 mm. The balls are placed on a stand of 17 mm height. Angular velocity of the link is 1.2 rad/s.

The flight distance of the balls are measured. The mean value of the data are taken after five measurements for each stiffness condition, which is shown in Table III.

For both cases, the balls fly farther if the stiffness of the VSJ is maximum. The golf ball flies 43 mm farther when the stiffness is maximum. The table-tennis ball flies 104 mm farther when the stiffness is maximum. Since the mass of the balls does not change and the ball rests before hitting, the experiment shows that the acceleration of the balls after collision is affected by different stiffness. Less stiffness results in less acceleration of the balls, which implies collision with less stiffness is safer.

V. CONCLUSION

A robot joint with variable stiffness was presented. Compliance was generated by leaf springs attached to the rotational axis. Changing the effective length of the springs resulted in changes in stiffness of the springs. The effective length of the springs were changed via moving the slider, which had rollers sled on the spring. The sliders were moved with four-bar linkage. Two identical actuators were connected to the four-bar linkage resulting in parallel actuation. Due to parallel actuation, the load to the VSJ was shared by the actuators. Furthermore, no torque was required by the actuators to maintain the stiffness constant, which implies better energy efficiency. When the bars rotated at the same speed in the same direction, the axis rotates without changing the location of the sliders, which resulted in the stiffness being unchanged. When the bars rotated in the opposite directions, the sliders moved while the axis

remain motionless, which resulted in change in stiffness of the joint. A nonlinear controller was suggested and proven to be a stabilizing controller using a singular perturbation model. The controller assumed the actuators were identical, which was not true in the implemented system. Asymmetries and uncertainties in model parameters resulted in nonzero steady-state errors, which should be further investigated in order to reduce the effects of them. Experiments were conducted to show that the position and stiffness of the joint were controlled independently using two actuators. The stiffness was changed much faster than the position of the link and vibration occurred with minimum stiffness. When a ball was hit by the link attached to the VSJ with maximum stiffness, the ball flew farther than when the stiffness was minimum. Since the safety of the object depends on the acceleration after the collision, the experiment showed that having a less stiff joint was safer in case of an unexpected collision with humans. A manipulator of a service robot can be equipped with the VSJ to prevent damage to humans when an unexpected collision occurs.

APPENDIX

PROOF OF THE EXPONENTIAL STABILITY OF THE REDUCED MODEL

Proof: Since $\sigma(\zeta_f) > 0$, and $J_l > 0$, κ_0 is positive. The dynamics of the reduced system with the control (14) is given by

$$\dot{\zeta}_2^s = -2\lambda\zeta_2^s + \lambda\zeta_3^s - \left(1 + \frac{\lambda^2}{\kappa_0}\right)\dot{\zeta}_3^s \tag{25}$$

$$\ddot{\zeta}_3^s = -\kappa_0\zeta_3 + \kappa_0\zeta_2. \tag{26}$$

Letting a candidate Lyapunov function be defined as

$$V = \frac{\kappa_0}{2}\xi^2 + \frac{\kappa_0}{2}\zeta_3^2 + \frac{1}{2}\dot{\zeta}_3^2 \tag{27}$$

where $\xi = \zeta_2^s + (\lambda/\kappa_0)\dot{\zeta}_3^s$, then the candidate Lyapunov function is positive, except for $\zeta_2^s = \zeta_3^s = \dot{\zeta}_3^s = 0$. The derivative of the control Lyapunov function is given by

$$\begin{aligned}
\dot{V} &= \kappa_0\xi\dot{\xi} + \kappa_0\zeta_3\dot{\zeta}_3 + \dot{\zeta}_3\ddot{\zeta}_3 \\
&= \kappa_0\xi\dot{\xi} + \dot{\zeta}_3^s(\kappa_0\xi - \lambda\dot{\zeta}_3^s) \\
&= -\lambda(\dot{\zeta}_3^s)^2 + \xi(\kappa_0\dot{\xi} + \kappa_0\dot{\zeta}_3^s) \\
&= -\lambda(\dot{\zeta}_3^s)^2 + \kappa_0\xi\left(-\lambda\zeta_2^s - \frac{\lambda^2}{\kappa_0}\dot{\zeta}_3^s\right) \\
&= -\lambda(\dot{\zeta}_3^s)^2 - \kappa_0\lambda\xi^2 \le 0.
\end{aligned} \tag{28}$$

Therefore, the reduced system is stable.

Letting $\Omega = \{\zeta^s \in \mathbb{R}^3 | \dot{V} = 0\}$, then

$$\Omega = \{\zeta^s \in \mathbb{R}^3 | \zeta_2^s = 0, \dot{\zeta}_3^s = 0\}. \tag{29}$$

Letting $M \subset \Omega$ be the largest invariant subset of Ω, then $M = \{\zeta^s \in \Omega | \zeta^s = [\zeta_2^s, \zeta_3^s, \dot{\zeta}_3^s]^T = 0\}$. Therefore, the system is asymptotically stable, which also implies that the system is exponentially stable since the system is linear.

REFERENCES

[1] B. R. Shetty and M. H. Ang, Jr., "Active compliance control of a PUMA 560 robot," in *Proc. IEEE Int. Conf. Robot. Autom.*, Minneapolis, MN, Apr. 1996, pp. 3720–3725.

[2] M. Zinn, B. Roth, O. Khatib, and J. K. Salisbury, "A new actuation approach for human friendly robot design," *Int. J. Robot. Res.*, vol. 34, no. 4–5, pp. 379–398, Apr./May 2004.

[3] D. Shin, I. Sardellitti, and O. Khatib, "A hybrid actuation approach for human-friendly robot design," in *Proc. IEEE Int. Conf. Robot. Autom.*, Pasadena, CA, May 2008, pp. 1747–1752.

[4] W. Wang, R. N. K. Loh, and E. Y. Gu, "Passive compliance versus active compliance in robot-based automated assembly systems," *Ind. Robot*, vol. 25, no. 1, pp. 48–57, 1998.

[5] R. Van Ham, T. G. Sugar, B. Vanderborght, K. W. Hollander, and D. Lefeber, "Compliant actuator designs," *IEEE Robot. Autom. Mag.*, vol. 16, no. 3, pp. 81–94, Sep. 2009.

[6] A. Bicchi, S. L. Rizzini, and G. Tonietti, "Compliant design for intrinsic safety: General issues and preliminary design," in *Proc. IEEE/RSJ Conf. Intell. Syst. Robots*, Maui, HI, Apr. 2001, pp. 249–254.

[7] A. De Luca and P. Lucibello, "A general algorithm for dynamic feedback linearization of robots with elastic joints," in *Proc. IEEE Int. Conf. Robot. Autom.*, Leuven, Belgium, May 1998, pp. 504–510.

[8] G. Palli, C. Melchiorri, and A. De Luca, "On the feedback linearization of robots with variable joint stiffness," in *Proc. IEEE Int. Conf. Robot. Autom.*, Pasadena, CA, May 2008, pp. 1753–1759.

[9] J. Choi, S. Park, W. Lee, and S. Kang, "Design of a robot joint with variable stiffness," in *Proc. IEEE Int. Conf. Robot. Autom.*, Pasadena, CA, May 2008, pp. 1760–1765.

[10] P. Tomei, "A simple PD controller for robotics with elastic joints," *IEEE Trans. Automat. Control*, vol. 36, no. 10, pp. 1208–1213, Oct. 1991.

[11] M. W. Spong, "Modeling and control of elastic joint robots," *J. Dyn. Syst., Meas., Control*, vol. 109, pp. 310–319, Dec. 1987.

[12] G. A. Pratt and M. M. Williamson, "Series elastic actuator," in *Proc. IEEE/RSJ Conf. Intell. Syst. Robots*, Pittsburgh, PA, Aug. 1995, pp. 399–406.

[13] R. V. Ham, B. Vanderborght, M. Van Damme, B. Verrelst, and D. Lefeber, "MACCEPA, the mechanically adjustable compliance and controllable equilibrium position actuator: Design and implementation in a biped robot," *Robot. Auton. Syst.*, vol. 55, pp. 761–768, 2007.

[14] J. W. Hurst, J. E. Chestnutt, and A. A. Rizzi, "An actuator with physically variable stiffness for highly dynamic legged locomotion," in *Proc. IEEE Int. Conf. Robot. Autom.*, New Orleans, LA, Apr. 2004, pp. 4662–4667.

[15] S. Wolf and G. Hirzinger, "A new variable stiffness design: Matching requirements of the next robot generation," in *Proc. IEEE Int. Conf. Robot. Autom.*, Pasadena, CA, May 2008, pp. 1741–1746.

[16] K. W. Hollander, T. G. Sugar, and D. E. Herring, "Adjustable robotic tendon using a 'Jack Spring,'" in *Proc. Int. Conf. Rehabil. Robot.*, Chicago, IL, 2005, pp. 113–118.

[17] T. Morita and S. Sugano, "Design and development of a new robot joint using a mechanical impedance adjuster," in *Proc. IEEE Int. Conf. Robot. Autom.*, Nagoya, Japan, May 1995, pp. 2469–2475.

[18] C. English and D. Russell, "Implementation of variable joint stiffness through antagonistic actuation using rolamite springs," *Mech. Mach. Theory*, vol. 34, pp. 27–40, 1999.

[19] S. A. Migliore, E. A. Brown, and S. P. DeWeerth, "Biologically inspired joint stiffness control," in *Proc. IEEE Int. Conf. Robot. Autom.*, Barcelona, Spain, Apr. 2005, pp. 4508–4513.

[20] G. Tonietti, R. Schiavi, and A. Bicchi, "Design and control of a variable stiffness actuator for safe and fast physical human/robot interaction," in *Proc. IEEE Int. Conf. Robot. Autom.*, Barcelona, Spain, Apr. 2005, pp. 526–531.

[21] R. Schiavi, G. Grioli, S. Sen, and A. Bicchi, "VSA-II: A novel prototype of variable stiffness actuator for safe and performing robots interacting with humans," in *Proc. IEEE Int. Conf. Robot. Autom.*, Pasadena, CA, May 2008, pp. 2171–2176.

[22] J. Choi, S. Hong, W. Lee, and S. Kang, "A variable stiffness joint using leaf springs for robot manipulators," in *Proc. IEEE Int. Conf. Robot. Autom.*, Kobe, Japan, May 2009, pp. 4363–4368.

[23] B. Vanderborght, R. Van Ham, D. Lefeber, T. G. Sugar, and K. W. Hollander, "Comparison of mechanical design and energy consumption of adaptable, passive-compliant actuators," *Int. J. Robot. Res.*, vol. 28, no. 1, pp. 90–103, Jan. 2009.

[24] S. H. Crandall, N. C. Dahl, and T. J. Lardner, *An Introduction to the Mechanics of Solids*, 2nd ed. New York: McGraw-Hill, 1978.

[25] P. Kokotović, H. K. Khalil, and J. O'Reilly, *Singular Perturbation Methods in Control: Analysis and Design*. Philadelphia, PA: Soc. Ind. Appl. Math., 1999.
[26] H. K. Khalil, *Nonlinear systems*, 2nd ed. Englewood Cliffs, NJ: Prentice-Hall, 1996.
[27] D. Vischer and O. Khatib, "Design and development of high-performance torque-controlled joints," *IEEE Trans. Robot. Autom.*, vol. 11, no. 4, pp. 537–544, Aug. 1995.
[28] D. W. Robinson, "Design and analysis of series elasticity in closed-loop actuator force control," Ph.D. dissertation, Mass. Inst. Technol., Cambridge, MA, Jun. 2000.
[29] H. Vallery, R. Ekkelenkamp, H. van der Kooij, and M. Buss, "Passive and accurate torque control of series elastic actuators," in *Proc. IEEE/RSJ Conf. Intell. Syst. Robots*, San Diego, CA, 2007, pp. 3534–3538.

Junho Choi (M'10) received the B.S. degree in electrical engineering from the Hanyang University, Seoul, Korea, in 2000, and the Ph.D. degree in electrical engineering systems from the University of Michigan, Ann Arbor, in 2005.

He is currently a Senior Research Scientist with the Korea Institute of Science and Technology, Seoul. His research interests include nonlinear control, bipedal robot control, manipulator control, and the design and control of a safe-joint for robot manipulators.

Seonghun Hong (S'10) received the B.S. degree in electrical and computer engineering in 2007 from Hanyang University, Seoul, Korea, where he is currently working toward the Ph.D. degree in electrical engineering.

He received the license of Secondary School Teacher (Class-II) with interest in the field of Education. Since 2007, he has been with the Center for Cognitive Robotics Research, Korea Institute of Science and Technology, Seoul. His current research interests include nonlinear systems, applications to robotic manipulation and field robots in the field of control engineering, cognitive science, and multiple intelligence in the field of education.

Woosub Lee received the B.S. degree in mechanical engineering from Sogang University, Seoul, Korea, in 1999, and the M.S. degree in electronic engineering from Yonsei University, Seoul, in 2004.

Since 2004, he has been a Research Scientist with the Korea Institute of Science and Technology, Seoul. His current research interests are the design and control of field robot systems and dependable manipulators.

Sungchul Kang (M'98) received the B.S., M.S., and Ph.D. degrees in mechanical design and production engineering from Seoul National University, Seoul, Korea, in 1989, 1991, and 1998, respectively.

Since 1991, he has been with Korea Institute of Science and Technology, Seoul, where he is currently a Principal Research Scientist. In 2000, he was a one-year Postdoctoral Researcher with the Mechanical Engineering Laboratory, Japan. In 2006, he was a Visiting Researcher with the Artificial Intelligence Laboratory, Stanford University, Stanford, CA. His current research interests include robot manipulation, haptic sensing and display, and field robot systems.

Munsang Kim (M'96) received the B.S. and M.S degrees in mechanical engineering from the Seoul National University, Seoul, Korea, in 1980 and 1982, respectively, and the Dr.-Ing. degree in robotics from the Technical University of Berlin, Berlin, Germany, in 1987.

Since 1987, he has been a Research Scientist with the Korea Institute of Science of Korea, Seoul, where he has been leading the Advanced Robotics Research Center since 2000 and has been the Director of the "Intelligent Robot—The Frontier 21 Program," since October 2003. His current research interests include the design and control of novel mobile-manipulation systems, haptic-device design and control, and sensor application to intelligent robots.